Intelligent sizing of a series hybrid electric power-train system based on Chaos-enhanced accelerated particle swarm optimization

Zhou, Quan; Zhang, Wei; Cash, Scott; Olatunbosun, Oluremi; Xu, Hongming; Lu, Guoxiang

Link to publication on Research at Birmingham portal

Intelligent Sizing of a Series Hybrid Electric Power-train System based on Chaos-enhanced Accelerated Particle Swarm Optimization

Quan Zhou[a], Wei Zhang[a], Scott Cash[a], Oluremi Olatunbosun[a], Hongming Xu[a, *], Guoxiang Lu[a]

a. Department of Mechanical Engineering, The University of Birmingham, Birmingham, B15 2TT, United Kingdom

Highlights

- A novel algorithm for hybrid electric powertrain intelligent sizing is introduced and applied.
- The proposed CAPSO algorithm is capable of finding the real optimal result with much higher reputation.
- Logistic mapping is the most effective strategy to build CAPSO.
- The CAPSO gave more reliable results and increased the efficiency by 1.71%.

Abstract

This paper proposes an intelligent sizing methodology to help engineers design the optimal series hybrid electric powertrain configuration. In the present work, the components sizing is formulated as a multi-objective optimization problem and the accelerated particle swarm optimization (APSO) algorithm is implemented as the computational intelligent solver. To further enhance the global optimal convergence performance, this paper introduces chaotic mapping strategies to tune the attraction parameter of APSO dynamically in each iteration. Firstly, the multi-objective optimization issue of intelligent sizing is formulated by modelling one case of a hybrid electric vehicle system for off-road application. The intelligent sizing mechanism based on APSO is then introduced, and 4 types of the most effective chaotic mapping strategy are investigated to upgrade the standard APSO into Chaos-enhanced Accelerated Particle Swarm Optimization (CAPSO) algorithm. The evaluation of the intelligent sizing systems based on standard APSO and CAPSOs are then performed. The Monte Carlo analysis and reputation evaluation indicate that the CAPSO outperforms the standard APSO for finding the real optimal sizing result with much higher reputation, and CAPSO with logistic mapping strategy is the most effective algorithm for HEV powertrain components intelligent sizing. In addition, this paper also performs the sensitivity analysis and Pareto analysis to help engineers customize the intelligent sizing system.

Keywords

- Hybrid Electric Powertrain;
- Intelligent Components Sizing;
- Multi-objective Optimization;
- Accelerated Particle Swarm Optimization;
- Chaos-enhanced Mapping Strategy;

---

* Corresponding Author: Email address: H.M.Xu@bham.ac.uk (H. Xu)

1. Introduction

The hybrid electric vehicle has been proposed as a promising alternative to the IC engine in tackling the energy consumption, environmental and global warming issues facing the automotive industry. Due to the increasingly stringent emission regulations (i.e. CO, CO_2, HC, NO_x, et al.) and the fierce competition between automotive manufacturers, hybrid electric vehicle's subsystems require hybrid components working more cooperatively to enhance the performance, i.e. hybrid propulsion systems [1], hybrid energy storage systems [2, 3], hybrid braking systems [4, 5], etc. Consequently, with the increasing number of hybrid components, traditional manual sizing methods are inefficient and hard to use in finding the real optimal solution, and engineers may even be confused about how to find an optimal configuration from variant topologies. Recently, intelligent sizing methods have emerged, and have been demonstrated as suitable for sizing and optimizing the vehicle system automatically.

Dynamic Programming (DP) is a very basic and commonly used intelligent methodology for solving the optimal process control problems in hybrid electric vehicle systems [6-8]. Although DP could always find the optimal global best solution by solving the nonlinear, non-convex models of the components consisting of continuous and integer optimization variables, DP has two main limitations which make DP an improper method for solving multi-variable and multi-objective components sizing problems. The biggest limitation of DP is that the computation time increases exponentially with the number of the components to be sized (input variables), and as a

50 consequence DP is usually used to deal with the optimal control issue which contains no more than two input
51 variables[9, 10]. The other limitation is that DP cannot directly include the component sizing into the optimization.
52 Instead, DP has to run in several loops to obtain the optimal control over a grid of component sizes[11].

53 Convex optimization[12] is another type of back-propagation intelligent method apart from DP. Convex
54 optimization is capable of overcoming the limitation of the size of state variables and obtain the global best solution
55 rapidly. However, engineers are required to have a very solid background in convex modelling and need to validate
56 that the optimization issue could be formulated into a convex model [13]. According to evidence of using convex
57 optimization to size hybrid electric vehicle components [13, 14], convex optimization cannot deal with integer
58 variables, however, in engineering practise, engineers are often required to find integer results, e.g. the number of
59 battery cells and the number of ultra-capacitor cells.

60 Solving the optimisation problems in automotive engineering using meta-heuristic algorithms is an emerging field
61 of study[15]. Compared with other metaheuristic algorithms (i.e. Genetic Algorithm [16], SPEA-II[17] , Artificial
62 Bees Algorithm [18], Ant Colony Algorithm[19], et al.), Particle Swarm Optimization (PSO) requires fewer
63 parameters to be tuned and less computational efforts for multi-objective optimization[20]. PSO also has the
64 capability of dealing with integer variables[14, 21] and is widely used in intelligent sizing and multi-objective
65 optimization in the automotive industry [21-26]. In order to accelerate PSO's convergence property, accelerated
66 particle swarm optimization (APSO) is proposed, and evidences have showed that optimizing HEV with standard
67 APSO outperforms the one with PSO [27, 28]. Nevertheless, in real engineering practice, similar to most
68 metaheuristic methods, APSO algorithm sometimes forces the agents to fall into local optima instead of global
69 optima. This phenomenon leads to divergent results when sizing the components using the same scenario at
70 different times; in other words, this phenomenon makes the sizing results inconsistent.

71 Recently, chaotic mapping strategies have emerged to enhance the chaos stability of metaheuristic algorithms [21,
72 29, 30]. The chaotic mapping is based on ergodicity, stochastic properties and regularity of the chaos. The chaotic
73 mapping could create some occasional 'accidents' or randomly accept some worse solution which could help the
74 stochastically created point in the main algorithm to escape from local optima [31]. Therefore, this paper proposes
75 an intelligent sizing methodology based on the Chaos-enhanced APSO (CAPSO), which uses chaotic mapping
76 strategy to tune the attraction parameter of APSO dynamically and obtains the optimal sizing result with higher
77 reputation. To evaluate the performance of the novel proposed method, this paper demonstrates the intelligent
78 sizing of a heavy-duty series hybrid electric vehicle as a case study.

79 The rest of this paper is structured as follows: in section 2, the intelligent sizing is designed as a multi-objective
80 optimization problem of choosing optimal combination of battery cell number, ultra-capacitor cell number and
81 engine displacement for a series hybrid electric vehicle. The present problem is formulated by modelling one case
82 study of sizing a series hybrid electric vehicle. Section 3 introduces the methodology of intelligent sizing using
83 APSO and CAPSOs. The performance of intelligent sizing methods is evaluated by Monte Carlo Analysis and
84 reputation evaluation in section 4. Section 4 also provides the sensitivity analysis and Pareto analysis of the
85 proposed system from data mining by CAPSO to help engineers customize the intelligent sizing system. Section 5
86 discusses the results and states the conclusions.

87 ## 2. Problem Formulation

88 ### 2.1 The System

89 This paper demonstrates sizing a heavy-duty series hybrid electric vehicle's powertrain presented in Figure 1. An

90   assumption is made that the optimal powertrain system topology is unknown before sizing and it will be determined

91   as 'triple power source', 'dual power source' or 'single source' depending on the sizing result, i.e. when the optimal

92   sizing result shows only battery and engine-generator are needed (when only the number of ultra-capacitor is zero),

93   the system will be with 'dual power source'.

94   The vehicle's power requirement property $P_{tm}(t)$ is firstly obtained from the simulation result of a forward-facing

95   fuzzy-logic driver driven vehicle model using the driving cycle profile provided by the customer. The vehicle is

96   modelled using a forward-facing approach as described by [32, 33], some basic parameters of the prototype vehicle

97   are listed in Table 1.The power supply system is modelled using a standard quasi-static backward-facing approach

98   as described in [22, 34]. Using the vehicle's power requirement property $P_{tm}(t)$ as the input of different power

99   storage system topologies, the overall energy efficiency and total components volume occupied are calculated with

100   scalable components over the same duty cycle.

101   **Table 1.** Basic Parameters of the Case Study Vehicle

Specification	*Value*	*Unit*
Vehicle Mass	*28*	*tone*
Radius of the wheels	*0.75*	*m*
Effective front Area	*7*	*m^2*
Maximum moving speed	*9.6*	*km/h*
Maximum towing load	*300*	*tone*

102   This paper mainly discusses the computational intelligent methodology to size the components intelligently and the

103   energy management strategy is simplified into a rule-based strategy to control the energy flow in the HESS system.

104   Nevertheless, the optimal control problems could also be solved together with the optimal component sizing as
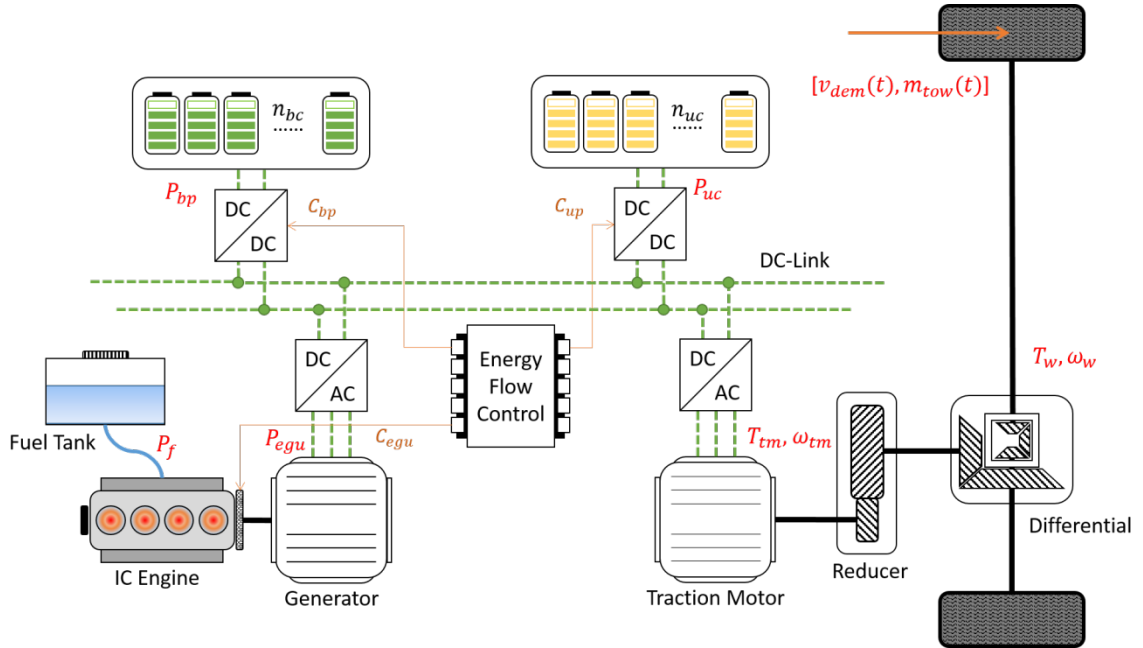
105   discussed by [13, 23, 35-37].

106

107   Figure 1. One case of the series hybrid electric powertrain

108　*2.1.1 Components Scaling*

109　The mathematical model of the three power system components subject to intelligent sizing must be scalable. The
110　scaling methodology of each power unit is described below.

111　The engine-generator unit (EGU) consists of an internal combustion engine, a generator and the fuel tank. The
112　engine model is based on a Williams approximation [26] and assumes a constant bore-to-stroke ratio. In this way,
113　the minimum fuel consumption and the most efficient power output could be scaled with the engine displacement
114　volume $V_{ice}(litre)$. The EGU's operating power could also be scaled with the engine power output using
115　look-up-table.

116　The battery package is made up with the battery cell type NCR-18650 series provided by Panasonic Automotive &
117　Industrial System Ltd.. The basic parameters of each individual cell could be found in [38]. The battery cell's I-V
118　dynamics is modelled with experimental data in [39] and constrained by the parameters provided. The voltage of
119　battery cells ranges from 2.5V to 4.2 V. The battery package parameters are obtained by arranging the battery cells
120　in parallel and series, therefore, the battery package is scaled by the total number of battery cells.

121　The ultra-capacitor package is made up with the ultra-capacitor cell type ESHSR-3000C0-002R7A5T series
122　provided by Nesscap Co Ltd., the basic parameters of each individual cell could be found in [40]. The
123　ultra-capacitor cell's I-V dynamics is modelled with experimental data in [21] and constrained by the parameters
124　provided. The maximum voltage of ultra-capacitor cell is 3.2V. The ultra-capacitor package parameters are obtained
125　by arranging the ultra-capacitor cells in parallel and series, therefore, the ultra-capacitor package is scaled by the
126　total number of ultra-capacitor cells.

127　*2.1.2 Power Flow Modelling and Control*

128　The power flow of the system is presented in Figure 2. In the system, the engine-generator can only send power to
129　the DC-link, the battery package and the ultra-capacitor package could both send and receive power from the
130　DC-link. The red arrow for battery and ultra-capacitor package show the direction of sending power, and the green
131　arrows represent the direction of receiving power from the DC-link. The traction motor takes power from the
132　DC-link to drive the vehicle, using the power requirement of the traction motor given by:

133
$$P_{link}(t) = \frac{P_{tm}(t)}{\eta_{tm}(T_{tm}, \omega_{tm})}$$
(1)

134　In equation 1, η_{tm} is a 2-D look-up-table provided by the traction motor supplier, in which the efficiency of the
135　electric motor could be obtained at different torque-speed points. $P_{tm}(t)$ is the power profile demand from the
136　customer's driving cycle. From the point of view of power balance, the power flow in the DC-link obeys:

137
$$P_{link}(t) = P_{egu}(t) + P_{bp}(t) + P_{up}(t)$$
(2)

138　In equation 2, $P_{egu}(t)$ is the power provided by engine-generator union, $P_{bp}(t)$ is the power provided by battery
139　package, $P_{up}(t)$ is the power provided by ultra-capacitor package.

140　The energy flow control strategy is based on two modes, one is power supply control, another is energy storage
141　devices charging control. The power supply control is using the rule-based strategy based on the DC-link power
142　demand. The power distribution in different scenarios is shown in Table 2.
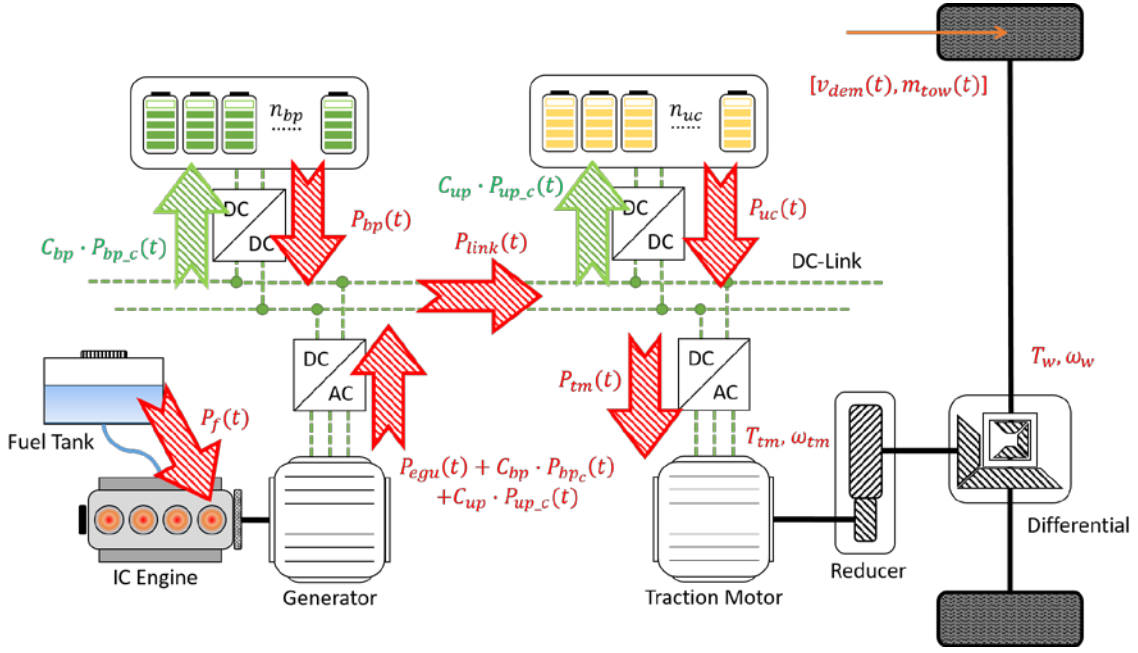
143

144   Figure 2. Power-flow model

145   **Table 2.** Power distribution in different scenarios

Scenarios	P_{bp}	P_{up}	P_{egu}
• If $P_{link}(t) < P_{bp_{ava}}(t) < P_{up_{ava}}(t)$; or $P_{up_{ava}}(t) < P_{link}(t) < P_{bp_{ava}}(t)$;	$P_{link}(t)$;	0;	0;
• If $P_{link}(t) < P_{up_{ava}}(t) < P_{bp_{ava}}(t)$; or $P_{bp_{ava}}(t) < P_{link}(t) < P_{up_{ava}}(t)$;	0;	$P_{link}(t)$;	0;
• If $P_{bp_{ava}}(t) < P_{up_{ava}}(t) < P_{link}(t) < P_{bp_{ava}}(t) + P_{up_{ava}}(t)$;	$P_{bp_{ava}}(t)$;	$P_{link}(t) - P_{bp_{ava}}(t)$;	0;
• If $P_{up_{ava}}(t) < P_{bp_{ava}}(t) < P_{link}(t) < P_{bp_{ava}}(t) + P_{up_{ava}}(t)$;	$P_{link}(t) - P_{up_{ava}}(t)$;	$P_{up_{ava}}(t)$;	0;
• If $P_{link}(t) > P_{bp_{ava}}(t) + P_{up_{ava}}(t)$.	$P_{bp_{ava}}(t)$;	$P_{up_{ava}}(t)$;	$P_{link}(t) - P_{bp_{ava}}(t) - P_{up_{ava}}(t)$;

146 In Table 1, $P_{bp_{ava}}(t)$ and $P_{up_{ava}}(t)$ are the current available power that could be provided by battery package and
147 ultra-capacitor package respectively. Both are a function of current SOC (or SOE) and current load current[19].

148 On the other hand, the energy storage device charging control is based on a standard thermostat strategy, which
149 could be found in many studies[41, 42]. The thermostat controller could be easily modelled using the 'relay'
150 module in MATLAB/Simulink by setting the upper threshold and lower threshold with respective SOC and SOE
151 values to ensure that enough voltage and current could be applied. In this demonstration. the battery starts charging
152 when SOC is lower than 30% and stops when SOC comes back to 80%, and the ultra-capacitor starts charging
153 when SOE is lower than 45% and stops charging when SOE comes back to 100%. When the battery package or
154 ultra-capacitor package needs to be charged, the controller will set $C_{bp} = 1$ or $C_{up} = 1$. On the contrary, when the
155 battery package and ultra-capacitor package no longer need to be charged, the value of C_{bp} and C_{up} will be set

156 back to 0.

157 When both the power supply and charge control are considered, the power flow within each component could be
158 calculated using the following equations. For the battery package:

$$n_{bc} \cdot P_{bc}(t) = P_{bp}(t) - C_{bp}(t) \cdot P_{bp\_c} \tag{3}$$

160 In equation 3, n_{bc} is the number of battery cells in the battery package, $P_{bp}(t)$ is the power supply from the
161 battery package, P_{bp_c} is the battery package charging power and C_{bp} is the battery charge command based on
162 the charge control. $P_{bc}(t)$ is the power output by the battery cell, and it could be determined by:

$$P_{bc}(t) = V_{bc\_oc}(SOC) \cdot I_{bc} - V_{bc\_loss}(SOC, I_{bc}) \cdot I_{bc} \tag{4}$$

164 In equation 4, $V_{bc\_oc}(SOC)$ is the open circuit voltage of the battery cell and it is a function of SOC, and
165 $V_{bc\_loss}(SOC, I_{bc})$ is the volatege drop in the resistor and capacitor element in the battery cells' relevant circuit [39].
166 I_{bc} is the battery cells current which may affect the battery cells' SOC [14].

167 For the ultra-capacitor package,

$$n_{uc} \cdot P_{uc}(t) = P_{bp}(t) - C_{up}(t) \cdot P_{up\_c} \tag{5}$$

169 In equation 5, n_{uc} is the number of ultra-capacitor cells in the battery package, $P_{up}(t)$ is the power supply from
170 the ultra-capacitor package, P_{up_c} is the ultra-capacitor package charging power and C_{up} is the ultra-capacitor
171 charge command based on the charge control. $P_{uc}(t)$ is the power output by the ultra-capacitor, and it could be
172 determined by:

$$P_{uc}(t) = V_{uc\_oc}(SOE) \cdot I_{uc} - V_{uc\_loss}(SOE, I_{uc}) \cdot I_{uc} \tag{6}$$

174 In equation 6, $V_{uc\_oc}(SOE)$ is the open circuit voltage of the ultra-capacitor and it is a function of SOE, I_{bc} is the
175 ultra-capacitor's current, and $V_{uc\_loss}(SOE, I_{bc})$ is the voltage drop in the resistor and capacitor element in the
176 ultra-capacitor's relevant circuit [21].

177 For the engine generator, the Williams approximation [26] method is used for modelling the engine generator union
178 for different EGU size, and the power flow of the EGU obeys:

$$\frac{dis_{ice}}{dis_{ice}^*} \cdot \dot{m}_f \cdot H_f \cdot \eta_{ice}^* \cdot \eta_{ge}^* = P_{egu}(t) + C_{bp}(t) \cdot P_{bp_c} + C_{up}(t) \cdot P_{up\_c} \tag{7}$$

180 In equation 7, dis_{ice} is the displacement of current engine size. dis_{ice}^* is the baseline engine size, while η_{ice}^* and
181 η_{ge}^* are the engine efficiency map and generator efficiency map for the EGU with the baseline engine. $\dot{m}_f$ is the
182 fuel consumption in kg/s, and H_f is the heat value of the fuel, i.e. for the diesel fuel, $H_f = 44 \times 10^6$J/kg [43].

2.2 Multi-Objective Optimization Problem

184 A lot of previous studies have reported hybrid electric vehicle components sizing in terms of fuel consumptions,
185 overall efficiency, and total cost, et al.[21, 22, 26, 44]. For most off-highway vehicle manufacturers, developing a
186 hybrid electric vehicle based on their existing vehicle platform could significantly save time and cost. As vehicle
187 hybridization always increases the overall volume of power system components when reducing the fuel
188 consumption, there is always a great challenge to convert a conventional vehicle into a hybrid one within the
189 limited space. Therefore, this paper majorly considers the trade-off problem of power conversion efficiency and
190 overall volume occupied. In addition, the number of battery cells and ultra-capacitor cells should be integer, and the
191 resolution of engine displacement is rounded to one decimal place in Litres. Therefore, the intelligent sizing should

192 be regarded as an integer variables multi-objective optimization.

2.2.1 Search Area and Constrain

194 The lower limitation is constrained based on the basic power demand and energy demand based on the custom
195 driving cycle. The upper limitation is set according to the custom requirements of the maximum overall cost,
196 maximum overall volume occupied and the maximum engine displacement. Therefore, for the given case study, the
197 search variable should obey:

$$
\begin{cases}
0 \leq n_{uc} \leq 150 \\
2500 \leq n_{bc} \leq 3000 \\
3 \leq dis_{ice} \leq 4 \\
n_{bc} \geq \max\left[\mathrm{ceil}\left(\frac{P_{max} - n_{uc} \cdot P_{ucn} \cdot \eta_{upn} - dis_{ice} \cdot P_{icel} \cdot \eta_{egu}}{P_{bcn} \cdot \eta_{bpn}}\right), \mathrm{ceil}\left(\frac{Q_{min} - n_{uc} \cdot Q_{ucn} \cdot \eta_{upn}}{Q_{bcn} \cdot \eta_{bpn}}\right)\right]
\end{cases}
\tag{8}
$$

199 In addition, as the dynamic performances of battery and ultra-capacitor cannot be predicted in the design stage,
200 some input variables may produce some results that cannot be accepted in the real practice (e.g. making battery
201 SOC or ultra-capacitor SOE lower than 0). The proposed intelligent sizing methodology would forward the output
202 calculated by these unacceptable inputs into a penalty process by setting the output variables "Not-a-Number".
203 Therefore, the unacceptable variables could be automatically ignored during the intelligent search process.

2.2.2 Cost Function

205 In the proposed intelligent sizing methodology, two main targets are mainly concerned, one is the overall efficiency
206 in the DC-link, another is the overall volume occupied by the hybrid electric driving system. The first optimization
207 target is defined as:

$$
J_1 = \frac{\int_{t_0}^{t_{end}} P_{tm}(t) \cdot dt}{\left(1 - SOC_{up}(end)\right) \cdot Q_{up} + \left(1 - SOC_{bp}(end)\right) \cdot Q_{bp} + \int_{t_0}^{t_{end}} dis_{ice} P_f(t) \cdot dt}
\tag{9}
$$

209 In equation 9, P_{tm} is the power supplied to the traction motor. The product of dis_{ice} and $P_f(t)$ is the equivalent
210 power of fuel consumed by the engine generator.· Q_{up} and Q_{bp} are the energy capacity of ultra-capacitor package
211 and battery package respectively.

212 Another optimization objective is the overall volume occupied by the hybrid system components, and it is defined
213 as:

$$
J_2 = n_{bc} \cdot vol_{bc} + n_{uc} \cdot vol_{uc} + dis_{ice} \cdot G_{egu}
\tag{10}
$$

215 Where: vol_{bc} and vol_{uc} are the volume of each battery cell and ultra-capacitor cell respectively. G_{egu} is a gain
216 value that is used to establish the relationship between engine displacement and the overall volume of engine
217 generator package. In the present work, the multi-objective optimization is formulated by using the weighted sum
218 method [22]. Therefore, the intelligent sizing problem is formulated as:

$$\min J(x) = (1 - w) \cdot \left(\frac{1}{J_1(x)}\right) / \left(\frac{1}{J_1^*}\right) + w \cdot J_2(x)/J_2^*, \qquad w \in [0,1]$$

$$s.t. \begin{cases} 0 \leq n_{uc} \leq 150 \\ 2500 \leq n_{bc} \leq 3000 \\ 3 \leq dis_{ice} \leq 4 \\ n_{bc} \geq \max[\text{ceil}\left(\frac{P_{max} - n_{uc} \cdot P_{ucn} \cdot \eta_{upn} - dis_{ice} \cdot P_{icel} \cdot \eta_{egu}}{P_{bcn} \cdot \eta_{bpn}}\right), \text{ceil}\left(\frac{Q_{min} - n_{uc} \cdot Q_{ucn} \cdot \eta_{upn}}{Q_{bcn} \cdot \eta_{bpn}}\right)] \end{cases} \qquad (11)$$

3. Methodology

3.1 Mechanism of APSO Algorithm for intelligent sizing
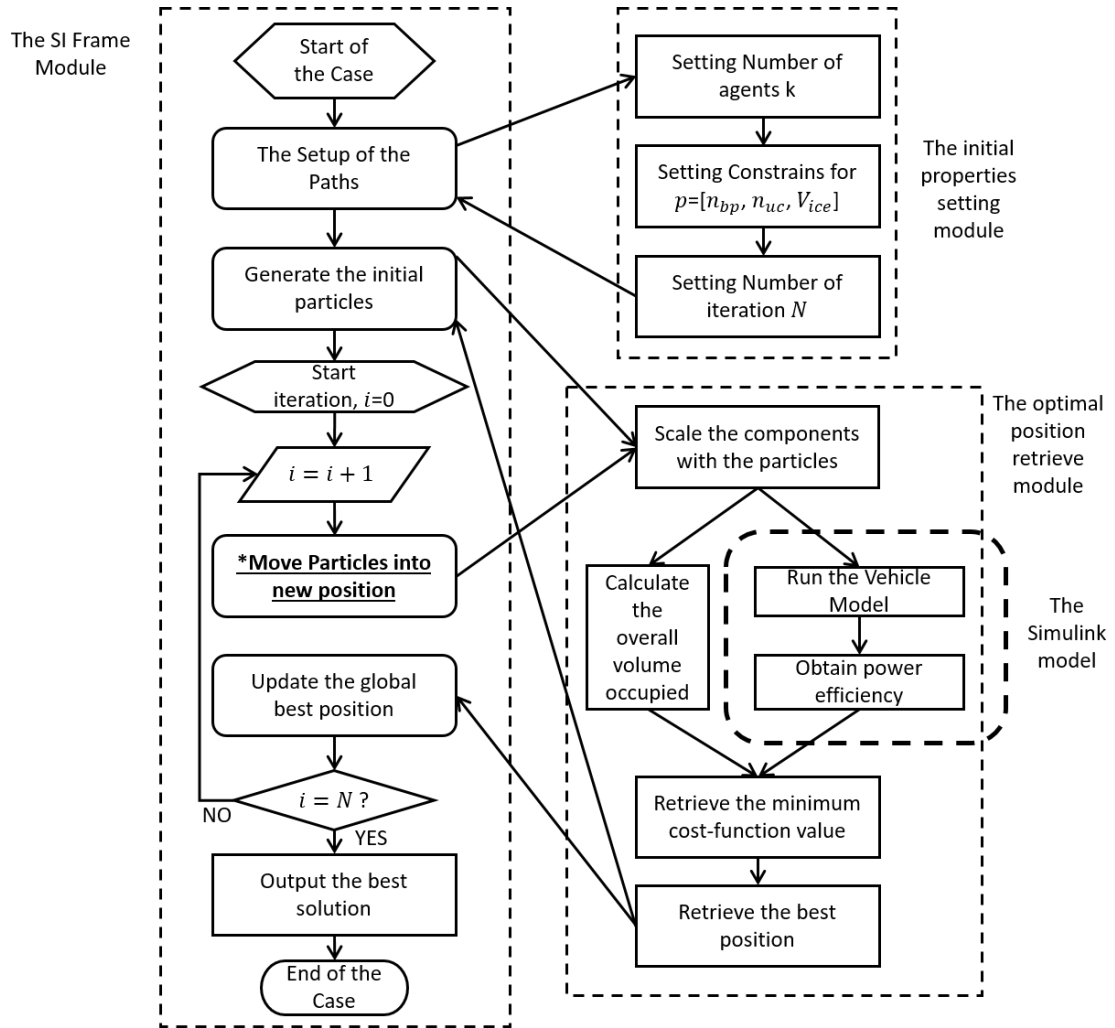
Figure 3. Flowchart for one intelligent sizing case based on Swarm Intelligent Algorithm

Accelerated Particle Swarm Optimization (APSO) algorithm [45], as an upgraded version of Particle Swarm Optimization (PSO), is also a computational algorithm inspired from animal swarms like ant colonies, bird flocks and fish schools and other biological features. Figure 3 provides the flow-chart of hybrid electric vehicle powertrain system intelligent sizing via APSO. Generally, a typical APSO mechanism consists of three main processes: Firstly, each particle or agent starts from an initial position chosen randomly within the search area subject to the

229   constraints. Using the initial position, the cost function value of each agent could be obtained using models or

230   real-world performance measurement. The optimal position of the initial positions could be found by retrieving the

231   position that achieved the optimal cost function value. Then, based on the agent's current position and the optimal

232   position of the initial particles, the position of each particles updates in each iteration. Each particle moved based

233   on three elements, namely, its current position, the best position in the swarm and a random factor. Finally, the

234   iteration ends when some of the pre-set criteria are achieved and the final optimal solution could be found in the

235   optimal solution of the last iteration.

236   In this present work, the position of each particle is defined as:

237
$$x^{(i,j)} = \begin{bmatrix} n_{uc}^{(i,j)} & n_{bc}^{(i,j)} & dis_{ice}^{(i,j)} \end{bmatrix} \tag{12}$$

238   In equation 12, the superscript i is the index of particle, for a swarm that has k particles, $i = [1,2,3 \dots k]$. The

239   superscript j is the index of iterations, for a SI algorithm that has N iterations, $j = [1,2,3 \dots N]$. $n_{uc}^{i,j}$, $n_{bc}^{i,j}$, and

240    $dis_{ice}^{i,j}$ are the number of ultra-capacitor cells, number of battery cells and the engine displacement of the EGU in

241   the ith agent and jth iteration.

242   For the APSO, the particles position updates with the following equation:

243
$$x^{(i+1,j)} = (1 - \beta) \cdot x^{(i,j)} + \beta \cdot g^{(*,j)} + \alpha^{(i)} \cdot r^{(i,j)} \tag{13}$$

244   In equation 13, $g^{(*,j)}$ is the global best position in the last iteration, β is the attraction parameters of APSO, α is

245   the convergence parameters of APSO that could be updated in each iteration as:

246
$$\alpha^{(i)} = \alpha^{(0)} \cdot \gamma^i \tag{14}$$

247   Evidence [20, 30] shows that for the standard APSO, the setting range of α_0 and γ are $\alpha^{(0)} \approx 0.5 \sim 1$, $\gamma \approx 0 \sim 1$.

248   In this paper, $\alpha^{(0)} = 0.9$ and $\gamma = 0.8$ are used for intelligent sizing.

249   ## 3.2 Chaotic Mapping Strategy

250   The value of β affects the APSO's convergence. When $\beta = 1$ in any step, the particles' convergence will remain

251   stationary even if current global best is not the true global best. On the other hand, when $\beta = 0$, the algorithm may

252   lead to slow changes. Therefore, in real practise, β needs to be well-tuned. The standard APSO usually keeps

253    $\beta = 0.5$ as a fixed value[20], although practice has suggested it could work efficiently, but the solutions are still

254   changing slightly as the optima are being approached. Therefore, a dynamic β value in each iteration is needed to

255   create some 'accidents', which could help the particles to jump out of the local optima convergence. Chaotic

256   mapping has been proposed to tune the β value. In this paper, 4 types of chaotic mapping strategies are introduced

257   to modify APSO, namely Gauss/mouse map, singer map, sinusoidal map and logistic map. The APSOs with the

258   proposed chaotic mapping strategies have been evaluated as the best 4 out of 12 candidates to solving the standard

259   algorithm testing functions (i.e. Griewank function, Ackley function, Sphere function)[30].

260   The map of each chaotic mapping strategy is modelled as follows:

261   *a)   Gauss/mouse map*

262   The following equations define the Gauss/mouse map [46]:

263
$$\beta^{(i+1)} = \begin{cases} 0 & \beta(i) = 0 \\ \frac{1}{\beta^{(i)}} mod(1) & otherwise \end{cases} \tag{15}$$

264 Where $mod(1)$ is the remainder of division of the number by 1 and the initial value $\beta(1) = 0.7$ is used for
265 simulation. In this paper, the CAPSO modified by Gauss/mouse map is named by CAPSO-I.

266 **b) Singer map**

267 Singer map is a one-dimensional system and is given below [47]:

268
$$\beta^{(i+1)} = \mu \cdot (7.86 \cdot \beta^{(i)} - 23.31 \cdot (\beta^{(i)})^2 + 28.75 \cdot \left(\beta^{(i)}\right)^3 - 13.302875 \cdot \left(\beta^{(i)}\right)^4) \tag{16}$$

269 Where $\mu = 0.95$ and the initial value $\beta^{(1)} = 0.7$ are used for simulation. In this paper, the CAPSO modified by
270 singer map is named by CAPSO-II.

271 **c) Sinusoidal map**

272 The sinusoidal map is mapped as [48]:

273
$$\beta^{(i+1)} = \sin(\pi \cdot \beta^{(i)}) \tag{17}$$

274 Where the initial value $\beta^{(1)} = 0.7$ is used for simulation. In this paper, the CAPSO modified by sinusoidal map is
275 named by CAPSO-III.

276 **d) Logistic map**

277 The logistic map [30] is represented by the following equation 18. The equation appears in nonlinear dynamics of
278 biological population evidencing chaotic behaviour.

279
$$\beta^{(i+1)} = a \cdot \beta^{(i)} \cdot (1 - \beta^{(i)}) \tag{18}$$

280 Where, the initial value $\beta^{(1)} = 0.7$ and $a = 4$ are used for simulation. In this paper, the CAPSO modified by
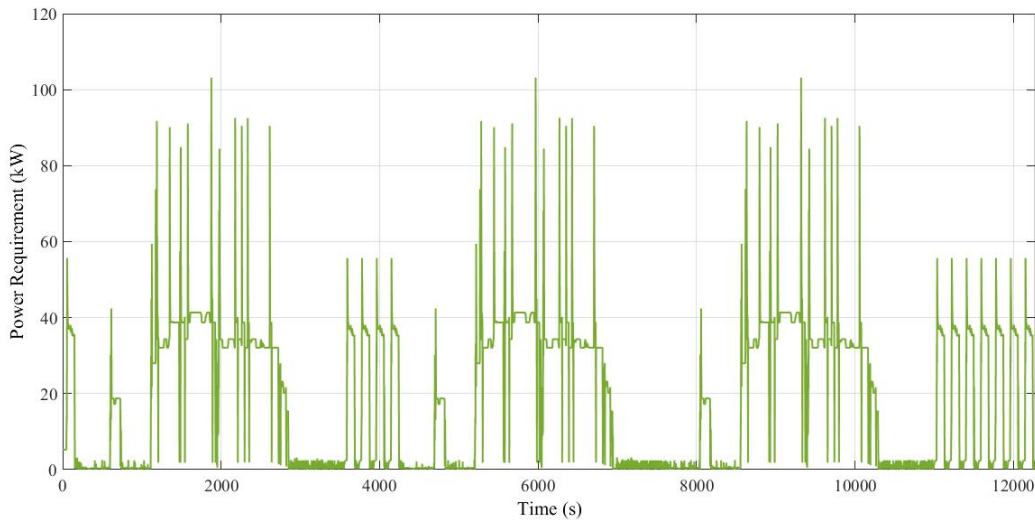281 Logistic map is named by CAPSO-IV.

282

283 Figure 4. Traction motor power consumption

11

284 ## 3.3 Co-simulation Set-up

285 *a) Driving cycle and power consumption profile*

286 Figure 4 represents the traction motor's power consumption property over the custom's driving cycle simulated by
287 the vehicle system model. Table 2 is a summary of the traction motor's power consumption profile

288 **Table 3.** Traction motor power consumption profile

Specification	Value	Unit
Cycle time	12,279	s
Peak power	103.1613	kW
Average power	18.9729	kW
Total energy	64.69	kWh

289 *b) Simple pseudo code of the intelligent sizing algorithm*

Intelligent Sizing via APSO or CAPSO

Load vehicle system parameters and driving cycle profile

APSO setting up

Setting fixed $\beta = 0.5$ or Mapping β with equation (15,16,17 or 18)

Initialize location $x^{(i,0)} = \begin{bmatrix} n_{uc}^{(i,0)} & n_{bc}^{(i,0)} & dis_{ice}^{(i,0)} \end{bmatrix}$ (i=1:k)of k particles

Simulate Vehicle system model

Find g^* at t=0

Start iteration...

For $j = 1:N$

    Update $\beta^{(i)}$ with equation (15,16,17 or 18) and current j

    Update location $x^{(i,j)} = \begin{bmatrix} n_{uc}^{(i,j)} & n_{bc}^{(i,j)} & dis_{ice}^{(i,j)} \end{bmatrix}$ of particles using equation (19) and $g^{(*,j-1)}$

    Simulate power system model

    Update $g^{(*,j)}$

End *for*

Output the final results $x^{(*,N)} = \begin{bmatrix} n_{uc}^{(*,N)} & n_{bc}^{(*,N)} & dis_{ice}^{(*,N)} \end{bmatrix}$

---

290 *c) Interface between the vehicle system and the algorithm*

291 Figure 5 presents the interface of the vehicle model with the intelligent sizing algorithm. In each iteration, the
292 inputs of the vehicle model are the number of ultra-capacitor cells, the number of battery cells, and the
293 displacement of internal combustion engine. All the inputs are k-dimension vectors, the vehicle model in Simulink
294 runs the simulation of n cases parallel in the same iteration and outputs the total efficiency and total volume
295 occupied. The outputs are also k-dimension vector, which are used to retrieve the best combination of components

296   size in this iteration and update the components size for the next iteration.
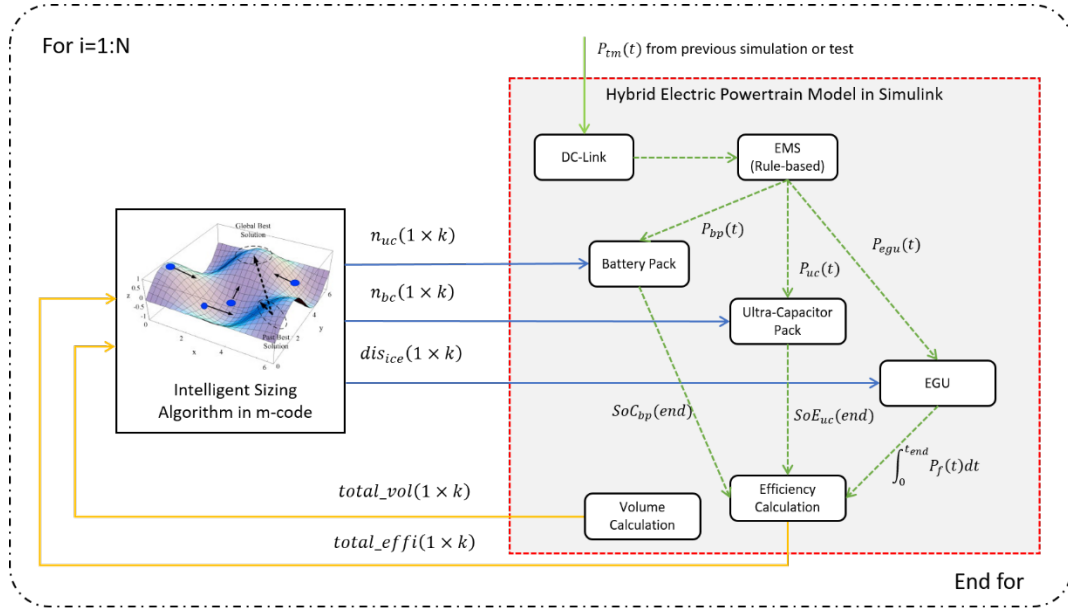

297

298   Figure 5. Interface of the vehicle model with the intelligent sizing algorithm
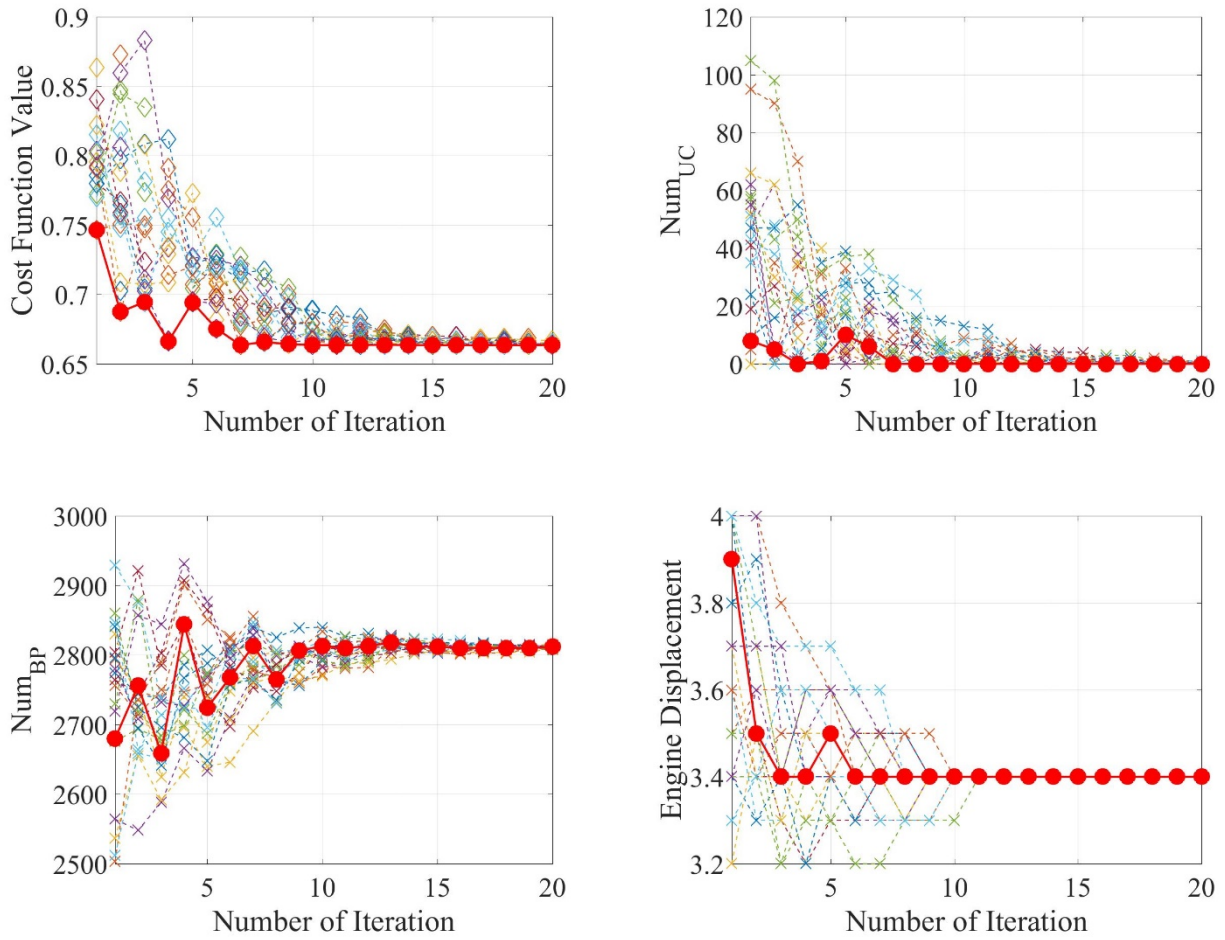

299   Figure 6. Sample of APSO based intelligent sizing (the red round points are the local optima in each iteration)

13

4. Results and Discussion

Figure 6 and Figure 7 present the evolution of one single swarm of standard APSO and APSO modified by logistic mapping strategy (CAPSO-IV). The weight value here is set to a fixed value of 0.5 to reflect an equal preference towards higher efficiency and lower volume occupied.

In each subplot of Figure 6 and Figure 7, the red round line is trajectories of the optimal value and respective optimal component size in each iteration while the other lines are the trajectories of other particles. From Figure 6 and Figure 7, both APSO and CAPSO have a good convergence performance within 20 iterations. The convergence speed has been increased by 5 times more than standard PSO[22]. From the single swarm calculation results, the CAPSO-IV outperforms APSO by achieving a better cost-function value. The evaluation of each swarm's coordinate (number of ultra-capacitor cells, number of battery cells, and displacement of ICE) indicated that CAPSO-IV might create some mutational position so that it has a wider search area than that of APSO, which is the reason why CAPSO-IV has a better probability of finding the global best solution than APSO. However, as both APSO and CAPSO-IV are stochastic search methods using a random number to generate and update each particle's position, the performance of APSO and CAPSO-IV cannot be fully evaluated by a single attempt. Thus, statistical measures based on several such samples must be taken to properly evaluate the performance of CAPSO-IV algorithm.
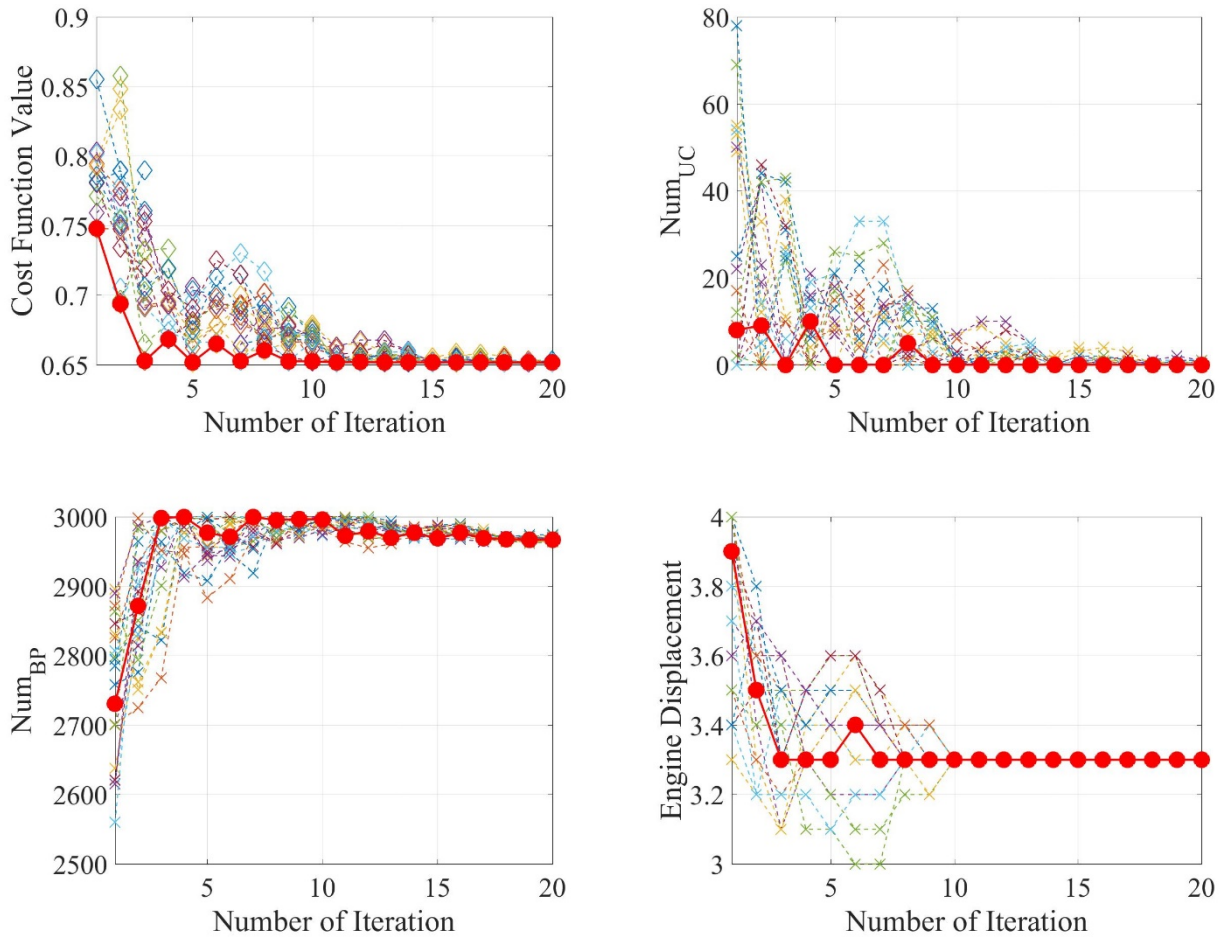

Figure 7. Sample of CAPSO-IV based intelligent sizing (the red round points are the local optima in each iteration)

4.1 Monte Carlo Analysis

For the purpose above, a Monte Carlo analysis is carried out to evaluate the performance of these algorithms. The standard APSO and CAPSO with 4 respective chaotic mapping strategies are each set-off 20 times with uniformly distributed random initial value.

Table 4. Mean value of 20 samples of standard APSO and each Chaos-enhanced APSOs

	Mean values $(\omega = 0.5)$				
	Standard APSO	*Gauss map*	*Singer map*	*Sinusoidal map*	*Logistic map*
J	*0.660729*	*0.660053*	*0.660063*	*0.657127*	*0.657006*
J_1	*45.41%*	*45.45%*	*45.76%*	*46.23%*	*46.18%*
J_2	*96.788*	*96.647*	*97.536*	*97.599*	*97.599*

Table 4 shows the resulting mean value of all the optimization objectives obtained by standard APSO and CAPSO. As the multi-objective optimization is to minimize the cost function value, all the CAPSOs were able to achieve a better mean value than APSO. Among all the CAPSOs, the logistic map strategy achieved the minimal cost function mean value. CAPSO reduced, by 0.56%, the mean value of the cost function calculated by standard APSO by increasing the total efficiency by 1.71% and the total volume by 0.83%.

Table 5. Standard deviation $\pm\sigma$ of 20 samples of standard APSO and each Chaos-enhanced APSOs

	Standard deviation $\pm\sigma$ $(\omega = 0.5)$				
	Standard APSO	*Gauss map*	*Singer map*	*Sinusoidal map*	*Logistic map*
J	*0.006538*	*0.006927*	*0.006771*	*0.006538*	*0.005939*
J_1	*0.0155*	*0.0175*	*0.0134*	*0.0147*	*0.0154*
J_2	*2.405*	*2.867*	*2.867*	*2.086*	*2.435*

Table 5 shows the resulting standard deviation of all the optimization objectives. The CAPSO by logistic mapping strategy is the only CAPSO that achieved lower standard deviation level of the cost function value than the standard APSO.

Therefore, from the Monte Carlo analysis, sizing the HEV components with the CAPSO mapped by logistic mapping strategy consistently locates a solution with lower cost function mean value and the standard deviation levels. In addition, evidence by statistics has indicated that CAPSO by logistic mapping strategy has more potential to find the global best than any other method.

4.2 Reputation Evaluation

In the Monte Carlo analysis, this paper evaluates each intelligent sizing method from the view of probability distribution. Nevertheless, in real practice, engineers are always concerned about the reputation of how an intelligent method achieves the real global best rather its mean value and standard deviation level. Therefore, we need a strict and observable method to evaluate the reputation of the proposed intelligent sizing method.
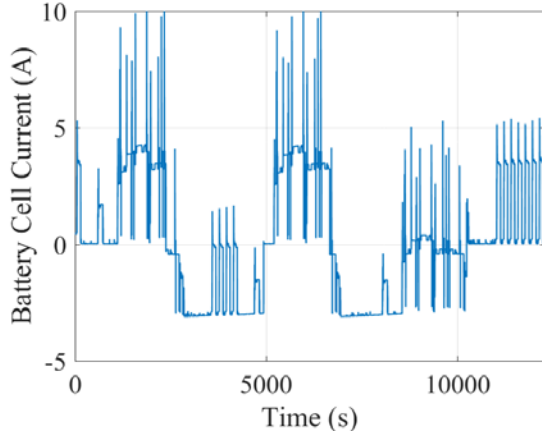
(a) Battery cell's current performance
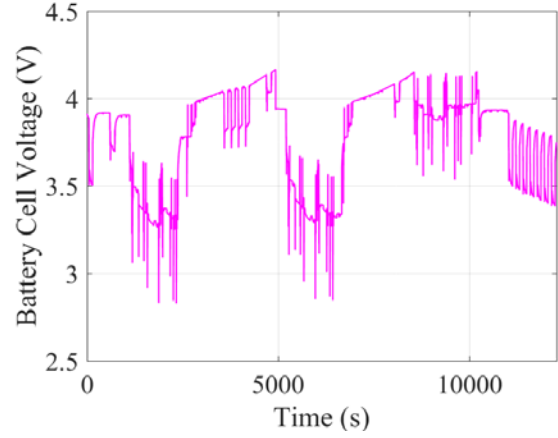
(b) Battery cell's voltage performance
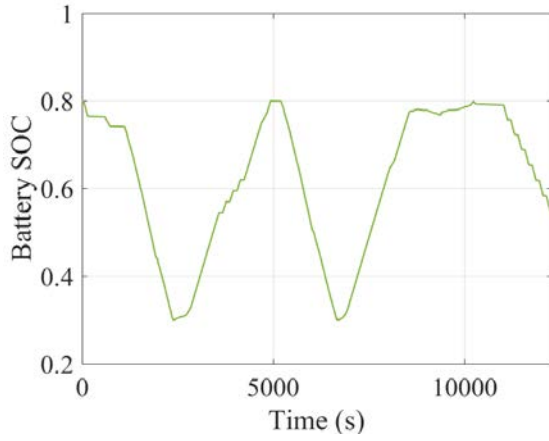
(c) Battery SOC
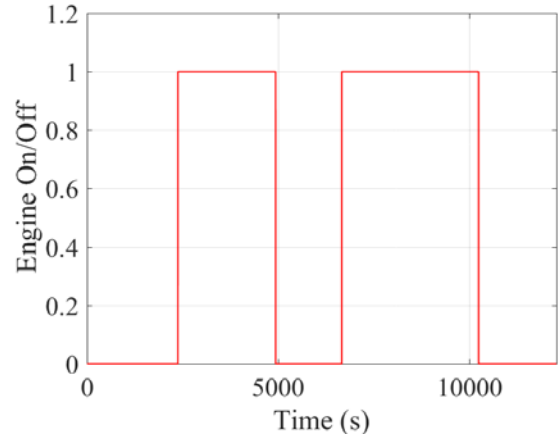
(d) Engine on/off command

340   Figure 8. Powertrain components' performance using the optimal sizing result

341   Table 6 shows the optimal results obtained by the standard APSO and CAPSOs, all of them could achieved same
342   optimal result. The result shows that the optimal system for the given duty cycle is a 'dual power source system'
343   including a battery package with 2976 battery cells and an engine-generator union with a 3.3 L diesel engine (no
344   ultra-capacitor is needed). The powertrain with the optimal components' sizes is than evaluated and the powertrain
345   performance is shown in Figure 8.

346   From Figure 8, the powertrain with the optimal components' sizes could work properly over the given duty cycle.
347   The battery could supply sufficient current and voltage during the duty cycle, and the engine-generator could
348   provide enough power for maintaining the battery SOC within the proper range as well as driving the vehicle.
349   Therefore, the sizing result is acceptable and could also be regarded as the 'global optimal sizing result'.

350   Then the reputational index is defined as,

351
$$R_i = \frac{Num_{opt.}}{Num_{all}} \tag{19}$$

352   Where, $Num_{opt.}$ is the number of the global optimal solutions of each algorithm and Num_{all} is the number of all
353   trials. Calculating by equation 19, the reputational index values of the standard APSO and CAPSOs are obtained in

354 Table 7.

355 **Table 6.** The optimal results of 20 samples of standard APSO and each CAPSOs ($w = 0.5$)

	Optimal Results	($w = 0.5$)			
	Standard APSO	Gauss map	Singer map	Sinusoidal map	Logistic map
J	0.651468	0.651468	0.651468	0.651468	0.651468
J_1	47.54%	47.54%	47.54%	47.54%	47.54%
J_2	99.309	99.309	99.309	99.309	99.309
n_{bc}	2967	2967	2967	2967	2967
n_{uc}	0	0	0	0	0
dis_{ice}	3.3	3.3	3.3	3.3	3.3

356 **Table 7.** Reputation index of APSO using standard value and four different chaotic maps

	Reputation Index				
	Standard APSO	Gauss map	Singer map	Sinusoidal map	Logistic map
$Num_{opt.}$	3	5	6	8	9
Num_{all}	20	20	20	20	20
R_i	0.15	0.25	0.30	0.40	0.45

357 From Table 4, Table 7 and Table 8, the algorithm with higher reputational index provides better performance in
358 terms of the mean value and worst results. Thus algorithms could be evaluated based on higher reputation. By
359 comparing the reputational index value, all the CAPSOs outperform the standard APSO. The CAPSO mapped by
360 logistic mapping strategy is the one, which has the highest reputational index value, and its reputational value is
361 200% higher than that of the standard APSO. Overall, we can suggest that the CAPSO mapped by logistic mapping
362 strategy is the most effective CAPSO for hybrid electric vehicle intelligent sizing.

363 **Table 8.** The worst results of 20 samples of standard APSO and each CAPSOs ($w = 0.5$)

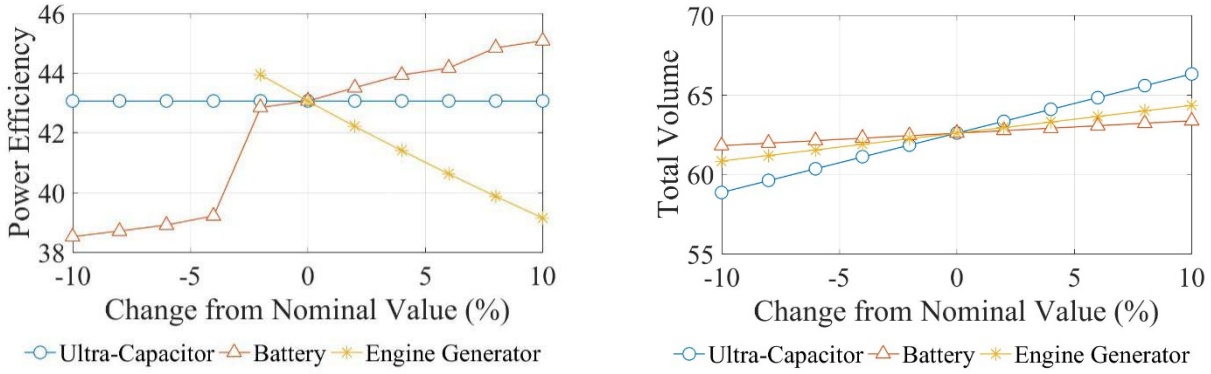|	Worst Results	($w = 0.5$)			
	Standard APSO	Gauss map	Singer map	Sinusoidal map	Logistic map
J	0.677074	0.677052	0.667052	0.665664	0.664475
J_1	42.78%	42.79%	42.79%	44.38%	45.13%
J_2	94.895	94.917	94.917	95.750	97.426
n_{bc}	2680	2681	2681	2763	2838
n_{uc}	0	0	0	0	0
dis_{ice}	3.5	3.5	3.5	3.4	3.4

4.3 Sensitivity Analysis

365   Figure 9.   Variation of the optimization objective values when changing the component size

366   The sensitivity analysis is performed to investigate the relative influence of the three parameters n_{bc}, n_{uc} and
367   dis_{ice} on the optimization objectives. The initial values of these three parameters are set using the mid-point values
368   in the search area defined in equation (11). Moreover, at each measurement, the selected parameter is increased by
369   2% of the initial value, while other parameters are kept constant. Figure 9 shows the variation of the power
370   efficiency and total volume while the selected parameters changed. The change of power efficiency indicates
371   increasing the number of battery cells and downsizing the engine could make a contribution to efficiency
372   development and the variation of number of ultra-capacitor cells does not have any significant contribution to
373   power efficiency.
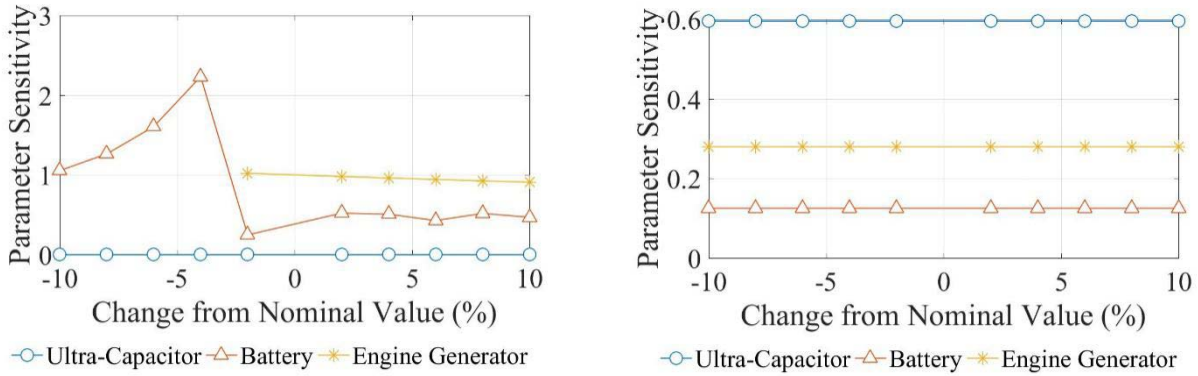
374   Figure 10.   Sensitivity of Ultra-capacitor cells' number, battery cells' number and engine displacement to the
375   optimization objectives

376   The sensitivity of each parameter to the optimization objectives could be calculated by [49]:

$$S_{\varepsilon,\delta} = \left| \frac{\Delta J_\delta / J_{\delta 0}}{\Delta x_\varepsilon / x_{\varepsilon 0}} \right| \tag{20}$$

378   Where $S_{\varepsilon,\delta}$ is the sensitivity of index to the selected parameters, ΔJ_δ is the variation of index, $\delta = 1$ or 2
379   represents the optimization objective. Δx_ε is the variation of the selected parameter, $\varepsilon = 1$, 2 or 3 represents the
380   selected parameter. $x_{\varepsilon 0}$ is the initial value of the parameters, and $J_{\delta 0}$ is the initial value corresponding to the

381 situation when $x_\varepsilon = x_{\varepsilon 0}$. The larger the sensitivity value, the more significant the effects of parameter on the
382 evaluation of total efficiency or total volume occupied.

383 From the results of sensitivity analysis shown in Figure 10, the values of sensitivity of the selected parameter to the
384 total volume keep constant while the parameters changes. Ultra-capacitor size is most sensitive to the volume and
385 battery size is the least sensitive one. The values of sensitivity of the selected parameter to the efficiency varies
386 while the selected parameters changes. The engine size is the most sensitive parameter while the ultra-capacitor
387 size is the least one.

388 Generally, in this given intelligent sizing issue, increasing the battery package size could make a contribution to
389 optimizing the total efficiency with least increase of total volume, reducing the engine size could make significant
390 contribution to increasing the efficiency and considerable volume reduction. Increasing the ultra-capacitor package
391 size does not make acceptable contribution to the efficiency optimization, whereas it may result in considerable
392 volume increase.

4.4 Pareto Analysis

394 In this paper, the intelligent sizing of hybrid electric vehicle is formulated into a multi-objective optimization
395 problem with a weight sum cost function in equation 11. The weight value $0 < w < 1$ determines the preference
396 of the objectives, namely, when $w = 0$, the intelligent sizing only seeks to maximise the efficiency, similarly, when
397 $w = 1$, the intelligent sizing only seeks to minimize the overall volume. Therefore, in this section, a Pareto analysis
398 is performed to investigate the influence of the weight value w on the trade-off of between maximizing the
399 efficiency and minimizing the volume.
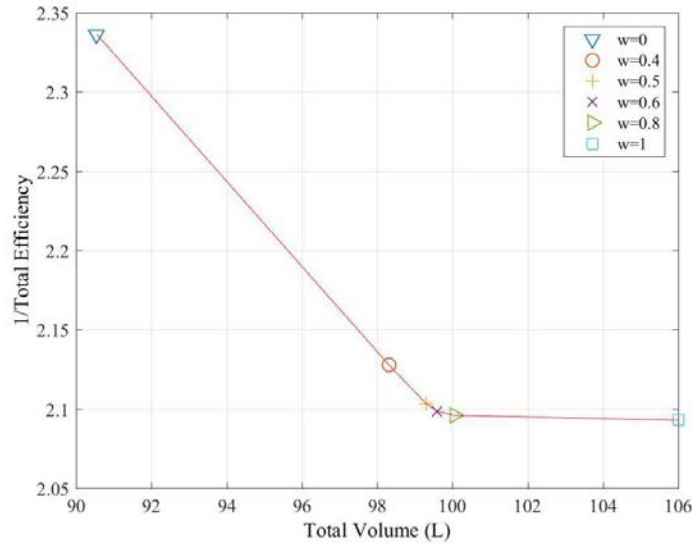
401 Figure 11. Pareto Frontier for different weight value settings (preference between volume and efficiency)

402 Figure 11 presents the Pareto optima frontier with different weight value. As can be seen, the total efficiency
403 increased by allowing the total volume to increase from the most effective configuration, i.e. from $w = 0$ to
404 $w = 0.4$. however, at some point, increasing the volume does not make any contribution to the efficiency
405 optimization, i.e. from $w = 0.8$ to $w = 1$. This trend is demonstrated in Figure 12, as can be seen, the increase in
406 total efficiency across w is around 11%. At the same time, the total volume has to increase around 15%.
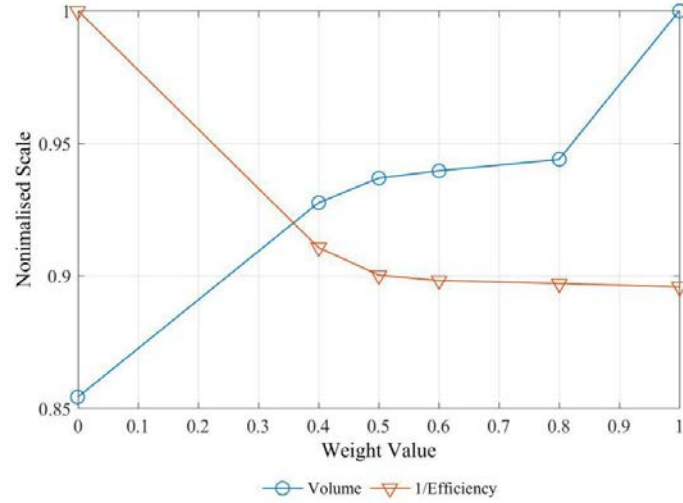
Figure 12. Effect of changing the weight value (preference between volume and efficiency)

Table 9 shows the objective values obtained by different weight values. In order to normalize the objective function values, this paper define the normalized gradient of each objective function value as:

$$
\begin{cases}
\Delta_1 = \dfrac{J_1^*}{\Delta J_1 \cdot \Delta w} \\
\Delta_2 = \dfrac{\Delta J_2}{J_2^* \cdot \Delta w}
\end{cases}
\tag{32}
$$

Where, J_1^* and J_2^* are maximum efficiency and maximum volume, ΔJ_1 and ΔJ_2 are the variation of the objective function value while the weight value is changing from 0.0 to 1.0. Δw is the variation of the weight value w. From Table 9, we can evaluate the effect of the weight value to the objective functions by evaluating the absolute value of the division of the normalized gradients. When changing the weight value from 0.4 to 0.5, the $|\Delta_1/\Delta_2|$ is the lowest, which means more rapid increase in efficiency with most acceptable increase in volume. When changing the weight value from 0.8 to 1.0, the $|\Delta_1/\Delta_2|$ is the highest, which means it is not cost-efficient with modest increase in the efficiency for such significant increase in volume.

Table 9. Numerical values of the Pareto set obtained using Chaotic APSO

	w value					
	0.0	*0.4*	*0.5*	*0.6*	*0.8*	*1.0*
J_1	*0.428*	*0.470*	*0.4754*	*0.4765*	*0.4771*	*0.4788*
J_2	*90.55*	*98.32*	*99.30*	*99.60*	*100.05*	*106.00*
Δ_1	*-*	*-0.2313*	*-0.1064*	*-0.0322*	*-0.0239*	*-0.2974*
Δ_2	*-*	*0.2453*	*0.1262*	*0.00257*	*0.0070*	*0.0082*
$|\Delta_1/\Delta_2|$	*-*	*0.9427*	*0.8433*	*1.2510*	*3.4146*	*36.3618*

5. Conclusions

The present work proposed an intelligent sizing method based on Chaotic-enhanced Accelerated Particle Swarm Optimization (CAPSO) and a demonstration on sizing a series hybrid electric powertrain was provided as a case

study. The major contribution of the present work is developing a reliable computational intelligent approach to help engineers determine the optimal vehicle powertrain configurations for particular uses. In this paper, 4 types of chaotic mapping strategy have been investigated to build up the CAPSO algorithm for intelligent sizing. The powertrain performance with the optimal components size has been investigated and sizing results by each algorithm have been evaluated. The conclusions drawn from the investigation are as follows:

1. The Monte Carlo Analysis indicates that the CAPSO based intelligent sizing results outperform the standard APSO by achieving a lower mean value of the cost function.
2. A new concept of 'Reputational Index' has been proposed for assessing the performance of intelligent sizing algorithm and it is shown to have the ability to consistently find the global optimal solution.
3. Logistic mapping appears to be the most effective strategy for CAPSO which can achieve the lowest mean value and standard derivation of the cost function and it also leads to the highest Reputational Index value which is 200% higher compared with the standard APSO.
4. The sensitivity analysis suggests that for the energy efficiency of a hybrid powertrain, engine displacement is the most sensitive parameter whereas ultra-capacitor size is the least sensitive parameter. For the power system volume, battery size is the least sensitive parameter while ultra-capacitor size is the most sensitive parameter.
5. The Pareto analysis suggests that the most cost-efficient weighting value in the cost function for the trade-off between energy efficiency and total volume is 0.5.

Furthermore, in this present research, the energy-flow control is simplified as a rule-based strategy. However, the proposed vehicle system provided sufficient interfaces for further optimization via control strategy design. In terms of the multi-objective optimization, the proposed method above could also optimize component size for different objectives such as total cost, fuel consumption, etc.

Conflict of Interests

The authors declare no conflict of interests.

Acknowledgement

Reference

[1] T. Hutchinson, S. Burgess, and G. Herrmann, "Current hybrid-electric powertrain architectures: Applying empirical design data to life cycle assessment and whole-life cost analysis," *Applied Energy,* vol. 119, pp. 314-329, 2014.

[2] Z. L. Alireza Khaligh, "Battery, Ultracapacitor, Fuel Cell, and Hybrid Energy Storage Systems for Electric, Hybrid Electric, Fuel Cell, and Plug-In Hybrid Electric Vehicles: State of the Art," *IEEE Transactions on Vehicular Technology,* vol. 59, p. 9, July 2010.

459   [3]   M. Abu Mallouh, E. Abdelhafez, M. Salah, M. Hamdan, B. Surgenor, and M. Youssef, "Model development and
460   analysis of a mid-sized hybrid fuel cell/battery vehicle with a representative driving cycle," *Journal of Power*
461   *Sources,* vol. 260, pp. 62-71, 2014.

462   [4]   B. Wang, X. Huang, J. Wang, X. Guo, and X. Zhu, "A robust wheel slip ratio control design combining
463   hydraulic and regenerative braking systems for in-wheel-motors-driven electric Vehicles," *Journal of the*
464   *Franklin Institute,* vol. 352, pp. 577-602, 2015.

465   [5]   Q. Zhou, G. Tan, X. Guo, Z. Fang, and B. Gong, "Relationship between Braking Force and Pedal Force of a
466   Pedal Controlled Parallelized Energy-Recuperation Retarder System," *SAE Technical Paper 2014-01-1783,* vol.
467   1, 2014.

468   [6]   B.-C. Chen, Y.-Y. Wu, and H.-C. Tsai, "Design and analysis of power management strategy for range extended
469   electric vehicle using dynamic programming," *Applied Energy,* vol. 113, pp. 1764-1774, 2014.

470   [7]   G. Jianping, S. Fengchun, H. Hongwen, Z. Guoming G., and S. Elias G., "A Comparative Study of Supervisory
471   Control Strategies for a Series Hybrid Electric Vehicle," presented at the Power and Energy Engineering
472   Conference, 2009. APPEEC 2009. Asia-Pacific, Wuhan, China, 2009.

473   [8]   J. P. Gao, G. M. G. Zhu, E. G. Strangas, and F. C. Sun, "Equivalent fuel consumption optimal control of a series
474   hybrid electric vehicle," *Proceedings of the Institution of Mechanical Engineers, Part D: Journal of Automobile*
475   *Engineering,* vol. 223, pp. 1003-1018, 2009.

476   [9]   Z. Song, H. Hofmann, J. Li, X. Han, and M. Ouyang, "Optimization for a Hybrid Energy Storage System in
477   Electric Vehicles using Dynamic Programing Approach," *Applied Energy,* vol. 139, pp. 151-162, 2015.

478   [10]   L. Xu, C. D. Mueller, J. Li, M. Ouyang, and Z. Hu, "Multi-objective component sizing based on optimal energy
479   management strategy of fuel cell electric vehicles," *Applied Energy,* vol. 157, pp. 664-674, 2015.

480   [11]   H. Omar and M. Joeri Van, "Optimal Power Management and Powertrain Components Sizing of Fuel
481   Cell/Battery Hybrid Electric Vehicles based on Particle Swarm Optimisation," *Int. J. Vehicle Design,* vol. 58, p.
482   23, 2012.

483   [12]   B. Stephen and V. Lieven, *Convex Optimization*: Cambridge University Press, 2004.

484   [13]   N. Murgovski, L. Johannesson, J. Sjöberg, and B. Egardt, "Component Sizing of a Plug-in Hybrid Electric
485   Powertrain via Convex Optimization," *Mechatronics,* vol. 22, pp. 106-120, 2012.

486   [14]   M. Pourabdollah, E. Silvas, N. Murgovski, M. Steinbuch, and B. Egardt, "Optimal Sizing of a Series PHEV:
487   Comparison between Convex Optimization and Particle Swarm Optimization," *IFAC-PapersOnLine,* vol. 48, pp.
488   16-22, 2015.

489   [15]   M.-H. Tayarani-N, X. Yao, and H. Xu, "Meta-Heuristic Algorithms in Car Engine Design: A Literature Survey,"
490   *IEEE Transactions on Evolutionary Computation,* vol. 19, pp. 609-629, 2015.

491   [16]   M. Montazeri-Gh, A. Poursamad, and B. Ghalichi, "Application of Genetic Algorithm for Optimization of
492   Control Strategy in Parallel Hybrid Electric Vehicles," *Journal of the Franklin Institute,* vol. 343, pp. 420-435,
493   2006.

494   [17]   H. Ma, H. Xu, J. Wang, T. Schnier, B. Neaves, C. Tan*, et al.*, "Model-Based Multiobjective Evolutionary
495   Algorithm Optimization for HCCI Engines," *IEEE Transactions on Vehicular Technology,* vol. 64, pp.
496   4326-4331, 2015.

497   [18]   L. V. T. and N. N. V., "Bees-Algorithm-based Optimization of Component Size and Control Tratgy Parameters
498   for Parallel Hybrid Electric Vehicles," *International Journal of Automotive Technology,* vol. 13, p. 8, 2012.

499   [19]   A. Castaings, W. Lhomme, R. Trigui, and A. Bouscayrol, "Comparison of energy management strategies of a
500   battery/supercapacitors system for electric vehicle under real-time constraints," *Applied Energy,* vol. 163, pp.
501   190-200, 2016.

502   [20]   X.-S. Yang, *Nature-Inspired Optimization Algorithms*: ELSEVIER, 2014.

503   [21]   A. Ostadi and M. Kazerani, "A Comparative Analysis of Optimal Sizing of Battery-Only, Ultracapacitor-Only,
504   and Battery–Ultracapacitor Hybrid Energy Storage Systems for a City Bus," *IEEE Transactions on Vehicular
505   Technology,* vol. 64, p. 12, October, 2015 2015.

506   [22]   E. Soren, D. Christian, and G. Lino, "Particle swarm optimisation for hybrid electric drive-train sizing," *Int. J.
507   Vehicle Design,* vol. 58, p. 19, 2012 2012.

508   [23]   G. B., M. J. K., and S. D., "Combined power management_design optimization for a fuel cell_battery plug-in
509   hybrid electric vehicle using multi-objective particle swarm optimization," *International Journal of Automotive
510   Technology,* vol. 15, p. 10, 2014.

511   [24]   E. Ahmed Masmoudi, O. Hegazy, J. Van Mierlo, R. Barrero, N. Omar, and P. Lataire, "PSO algorithm‐based
512   optimal power flow control of fuel cell/supercapacitor and fuel cell/battery hybrid electric vehicles," *The
513   international journal for computation and mathematics in electrical and electronic engineering,* vol. 32, pp.
514   86-107, 2012.

515   [25]   W. J., Z. C.-H., and C. N.-X., "PSO Algorithm-based Parameter Optimization for HEV Powertrain and its
516   Control Strategy," *International Journal of Automotive Technology,* vol. 9, p. 7, 2008 2008.

517   [26]   J. M. Lujan, C. Guardiola, B. Pla, and A. Reig, "Cost of ownership-efficient hybrid electric vehicle powertrain
518   sizing for multi-scenario driving cycles," *Proceedings of the Institution of Mechanical Engineers, Part D:
519   Journal of Automobile Engineering,* vol. 230, pp. 382-394, 2015.

520   [27]   I. Rahman, P. M. Vasant, B. S. M. Singh, and M. Abdullah-Al-Wadud, "On the Performance of Accelerated
521   Particle Swarm Optimization for Charging Plug-in Hybrid Electric Vehicles," *Alexandria Engineering Journal,*
522   vol. 55, pp. 419-426, 2016.

523   [28]   I. Rahman, P. M. Vasant, B. S. M. Singh, and M. Abdullah-Al-Wadud, "Swarm Intelligence based
524   State-of-Charge Optimization for Charging Plug-in Hybrid Electric Vehicles," *Energy and Sustainability V:
525   Special Contributions,* vol. 206, pp. 261-271, 2015.

526   [29]   X. Wu, B. Cao, X. Li, J. Xu, and X. Ren, "Component sizing optimization of plug-in hybrid electric vehicles,"
527   *Applied Energy,* vol. 88, pp. 799-804, 2011.

528   [30]   A. H. Gandomi, G. J. Yun, X.-S. Yang, and S. Talatahari, "Chaos-enhanced accelerated particle swarm
529   optimization," *Communications in Nonlinear Science and Numerical Simulation,* vol. 18, pp. 327-340, 2013.

530   [31]   Y.-Z. Luo, G.-J. Tang, and L.-N. Zhou, "Hybrid Approach for Solving Systems of Nonlinear Equations using
531   Chaos Optimization and Quasi-Newton Method," *Applied Soft Computing,* vol. 8, pp. 1068-1073, 2008.

532   [32]   K. B. Jeonghoon Song, "Performance evaluation of traction control systems using a vehicle dynamic model,"
533   *Proceedings of the Institution of Mechanical Engineers, Part D: Journal of Automobile Engineering,* vol. 218, p.
534   12, 2004.

535 [33] J. Liu, "Modeling, Configuration and Control Optimization of Power-split Hybrid Vehicles," Ph.D., The
536   University of Michigan, The University of Michigan, Michigan, USA, 2007.

537 [34] L. Guzzella and A. Sciarretta, *Vehicle Propulsion Systems: Introduction to Modeling and Optimization*. Berlin,
538   Germany: Springer-Verlag Berlin Heidelberg, 2013.

539 [35] R. Xiong, H. He, and F. Sun, "Methodology for Optimal Sizing of Hybrid Power System Using particle Swarm
540   Optimization and Dynamic Programming," *Energy Procedia,* vol. 75, pp. 1895-1900, 2015.

541 [36] Z. Xiaowu, H. Peng, and J. Sun, "A Near-Optimal Power Management Strategy for Rapid Component Sizing of
542   Multimode Power Split Hybrid Vehicles," *IEEE Transactions on Control Systems Technology,* vol. 23, p. 10,
543   March, 2015 2015.

544 [37] S.-Y. Chen, Y.-H. Hung, C.-H. Wu, and S.-T. Huang, "Optimal energy management of a hybrid electric
545   powertrain system using improved particle swarm optimization," *Applied Energy,* vol. 160, pp. 132-145, 2015.

546 [38] (2016). *Lithium   Ion   Batteries: Cylindrical   Type*.   Available:
547   https://eu.industrial.panasonic.com/products/batteries-energy-products/secondary-batteries-rechargeable-batterie
548   s/lithium-ion-batteries/series/cylindrical-type/ACI4002?reset=1

549 [39] M. Chen and G. A. Rincon-Mora, "Accurate Electrical Battery Model Capable of Predicting Runtime and I–V
550   Performance," *IEEE Transactions on Energy Conversion,* vol. 21, pp. 504-511, 2006.

551 [40] (2014). *Nesscap Electric Double Layer Capacitor, Large Cylindrical Weldable*. Available:
552   http://www.nesscap.com/ultracapacitor/EDLC/Supercapacitor/Large_cell_supercapacitor_family/cylindrical_su
553   percapacitor_cell.jsp

554 [41] Z. Song, H. Hofmann, J. Li, J. Hou, X. Han, and M. Ouyang, "Energy management strategies comparison for
555   electric vehicles with hybrid energy storage system," *Applied Energy,* vol. 134, pp. 321-331, 2014.

556 [42] E. Mehrdad, G. Yiming, and E. Ali, *Modern Electric, Hybrid Electric, and Fuel Cell Vehicles: Fundamentals,*
557   *Theory, and Design*: CRCP Press, Taylor & Francis Group, 2010.

558 [43] R. Isermann, *Engine Modeling and Control*. Berlin: Springers Berlin Heidelberg, 2014.

559 [44] Z. Song, J. Li, X. Han, L. Xu, L. Lu, M. Ouyang, *et al.*, "Multi-objective Optimization of a Semi-active
560   Battery/Supercapacitor Energy Storage System for Electric Vehicles," *Applied Energy,* vol. 135, pp. 212-224,
561   2014.

562 [45] X.-S. Yang, S. Deb, and S. Fong, "Accelerated Particle Swarm Optimization and Support Vector Machine for
563   Business Optimization and Applications," in *Networked Digital Technologies: Third International Conference,*
564   *NDT 2011, Macau, China, July 11-13, 2011. Proceedings*, S. Fong, Ed., ed Berlin, Heidelberg: Springer Berlin
565   Heidelberg, 2011, pp. 53-66.

566 [46] H. Di, H. Chen, J. Ling-Ge, Z. Hong-Wen, and H. Guang-Rui, "Chaotic characteristics of a one-dimensional
567   iterative map with infinite collapses," *IEEE Transactions on Circuits and Systems I: Fundamental Theory and*
568   *Applications,* vol. 48, pp. 900-906, 2001.

569 [47] I. Fister, M. Perc, S. M. Kamal, and I. Fister, "A review of chaos-based firefly algorithms: Perspectives and
570   research challenges," *Applied Mathematics and Computation,* vol. 252, pp. 155-165, 2015.

571 [48] Y. Li, S. Deng, and D. Xiao, "A novel Hash algorithm construction based on chaotic neural network," *Neural*
572   *Computing and Applications,* vol. 20, pp. 133-141, 2011.

573   [49]   Q. Zhou, X. Guo, G. Tan, X. Shen, Y. Ye, and Z. Wang, "Parameter Analysis on Torque Stabilization for the
574   Eddy Current Brake: A Developed Model, Simulation, and Sensitive Analysis," *Mathematical Problems in*
575   *Engineering,* vol. 2015, pp. 1-10, 2015.

576